JOURNAL OF MATERIALS SCIENCE 31 (1996) 2437–2441

Thermal shock behaviour of a coarse grain porous alumina

Part II *Stress intensity factor and damage evaluation*

F. MIGNARD, C. OLAGNON, M. SAADAOUI, G. FANTOZZI
Laboratoire GEMPPM, URA CNRS 341, bât. 502, INSA de Lyon, 20 bd. A. Einstein, 69621 Villeurbanne Cedex, France

The detailed analysis of the temperature field during thermal shock of an alumina specimen presented in Part I [1] is used to evaluate the transient stress field. The dependence with temperature of the elastic constants has been taken into account. After showing that the tensile stress is maximum at the centre of the largest specimen face, the transient stress intensity factor has been calculated. The flaw distribution and the critical stress intensity factor have been measured and reported on the stress intensity factor calculation. The experimental results in terms of thermal shock resistance have been compared to the theoretical prediction. The good correlation observed here suggests that a fine description of the thermal shock test and damage behaviour can be done.

1. Introduction

A thermal shock device with precise thermal boundary conditions has been previously presented in Part I [1]. The transient temperature field at any location of a coarse grain alumina specimen was evaluated from the cooling kinetics and the thermal properties of the material. The aim of this paper is to compare the thermal shock behaviour of the same alumina with a theoretical analysis. The stress field $\sigma(x, y, t)$ and the stress intensity factor $K(y, t)$ induced by thermal shock are evaluated from the temperature field $T(x, y, t)$ and from the elastic properties of the material. These elastic properties were measured as a function of temperature. Experimental results are compared to numerical calculations in order to present a global analysis of the alumina thermal shock behaviour.

2. Experimental procedure

2.1. Mechanical properties

As in part I [1], rectangular flexure specimens ($4 \times 6 \times 40\ mm^3$) were used as the basis for mechanical properties measurements. The dynamic elastic modulus was evaluated from the flexural resonance frequency. The bar specimen held by two wires was free from vibration and set in a furnace. This equipment allowed dynamic elastic modulus measurements from room temperature up to 1000 °C in air. Before conducting the room temperature measurements, the specimens were left for 24 h at 50 °C in a drying oven in order to eliminate room humidity from porosity and to work with standard conditions. Poisson's ratio was determined from longitudinal and lateral velocities of ultrasonic wave propagation experiments at room temperature. Flexural strengths were measured on thermally shocked and as received specimens with a universal testing machine (Schenck Treble RM-T 25). Tests were carried out with a four-point alumina device with an outer span of 35 mm and an inner span of 10 mm. The displacement rate was of $5\ mm\ s^{-1}$. Flexural strength, toughness and resistance to crack propagation have been measured from room temperature to 1000 °C in air. Toughness was determined using single edge notched beam (SENB) specimens with the equipment previously described. A 0.2 mm width notch was machined at a relative depth of 0.3. The displacement rate was also fixed at $5\ mm\ s^{-1}$. The measurements of the resistance to crack propagation were also conducted on the SENB specimen with imposed maximum deflection rate ($2.5\ \mu m\ min^{-1}$). The notch was again of 0.2 mm width but with a relative depth of about 0.6. The length of the crack was evaluated from the load–displacement curve by the compliance method.

2.2. Thermal shock tests

Thermal shock tests were conducted with the device previously described in Part I [1]. The characterization of the damage induced by thermal shock was done by measuring the evolution of the dynamic elastic modulus, the retained strength and the acoustic emission activity. Seventeen specimens were tested at different thermal shock temperatures.

3. Results

3.1. Mechanical properties

The evolution of the dynamic elastic modulus as a function of temperature is represented in Fig. 1. A linear decrease of the Young's modulus is observed

0022–2461

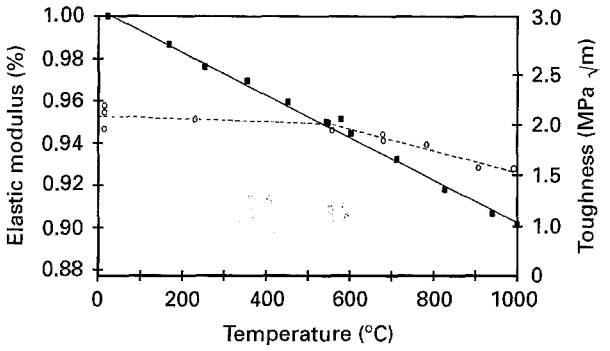

Figure 1 Evolution of dynamic elastic modulus (■) and toughness (○) of a coarse grain alumina as a function of temperature.

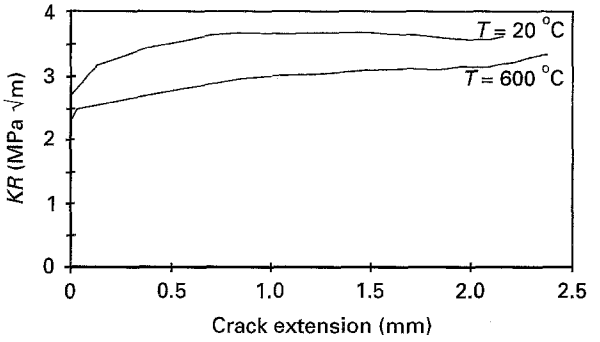

Figure 2 Resistance to crack propagation at room temperature and at 600 °C in air of a coarse grain alumina.

with increasing temperature up to a maximum variation of 10% at 1000 °C. These results are in agreement with those given by Watchman and Lam [2].

Poisson's ratio was found to be equal to $\nu = 0.2$ at room temperature. This provides a close fit with the value reported by Spriggs and Brissette [3]. They have expressed the Poisson's ratio of cold-pressed and sintered alumina as a function of porosity by the following equation: $\nu = 0.257 - 0.35P$, where P is the volume fraction of porosity. The Poisson's ratio was not studied as a function of temperature because Sakaguchi *et al.* [4] showed that this property was not dramatically thermally dependent.

Flexural strength measurements were conducted on 20 specimens at room temperature in air in order to obtain the defect size distribution in the material. In these conditions the mean flexural strength was found to be $\sigma_R = 131$ MPa with a standard deviation of 11 MPa. Despite the poor properties of this material a low scattering is observed. The flexural bending strength was also measured at 600 °C which corresponds to the temperature at the surface of the body at the instant of cracking for an initial thermal shock temperature difference of 682 °C. The mean strength was equal to $\sigma_R = 114 \pm 16$ MPa.

The evolution of the toughness with temperature is also represented in Fig. 1. A slight linear decrease is observed after above 600 °C. Note that these values are rather low for an alumina material. From the room temperature strength distribution and the value of toughness $K_{Ic} = 2 \pm 0.2$ MPa m$^{1/2}$, the initial critical defect size distribution was evaluated according to $K_{Ic} = Y(\frac{a}{w})\sigma_R a^{1/2}$, where $Y(\frac{a}{w})$ is given by Tada *et al.* [5]. The size was found to be in the range of 62 ± 10 μm to 86 ± 15 μm.

Owing to its coarse microstructure, this material might exhibit a rising R-curve behaviour. This R-curve was therefore measured at room temperature and at 600 °C in air (Fig. 2) which corresponds to the surface temperature of the specimen for a thermal shock at a critical temperature. There is however a modest R-curve behaviour of this alumina. The initial value of the stress intensity factor is of $KR_i = 2.7$ MPa m$^{1/2}$ at room temperature. A plateau value of $KR_i = 3.6$ MPa m$^{1/2}$ is reached for a crack extension of 0.7 mm. At 600 °C the R-curve effect of this material is less pronounced.

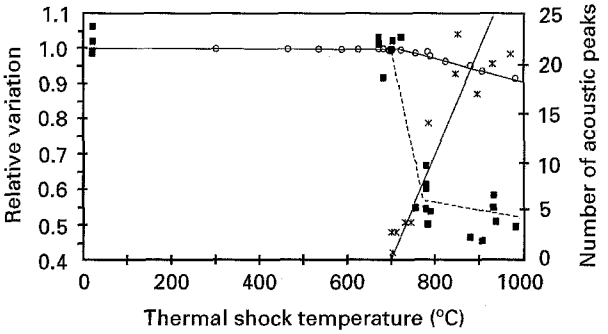

Figure 3 Evolution of the retained strength (■), modulus of elasticity (○) and acoustic emission (×) as a function of thermal shock temperature.

3.2. Thermal shock tests

Thermal shock degradation evaluated in terms of retained strength, number of acoustic peaks and variation of the dynamic elastic modulus are represented in Fig. 3. No evolution of these different properties was observed until a well defined step which characterizes a critical thermal shock temperature $T_c = 700$ °C. After this critical value, the dynamic Young's modulus decreases regularly while the retained strength shows a strong fall off followed by a plateau value. The high retained strength of this material is a characteristic of a refractory-like material, i.e. exhibiting a rapid decrease of the retained strength at the critical temperature difference but followed by a high plateau value of $\sigma_R = 0.5$. The appearance of the first acoustic peak is observed at the temperature difference where the retained strength and the dynamic Young's modulus decrease and corresponds to the maximum temperature difference between the core and the surface of the specimen as shown in Fig. 12 in Part I [1]. The number of acoustic peaks rises continuously with increasing temperature differences. The acoustic emission method allows the characterization of thermal shock damage and exhibits a fine correlation with other methods. This analysis by acoustic emission presents the advantages to give *in-situ* measurements and to be non-destructive. As mentioned in the first part, the precise time of appearance of the acoustic peaks could be determined. Different acoustic value collections recorded during thermal shock tests at various temperature differences are represented in Fig. 4. For all the tested temperature differences the duration of the acoustic emission

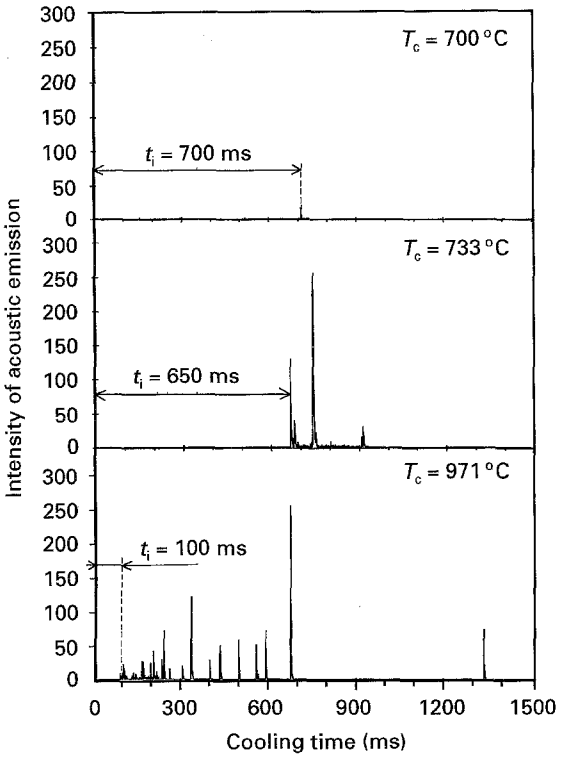

Figure 4 Acoustic value collection as a function cooling time for various thermal shock temperatures.

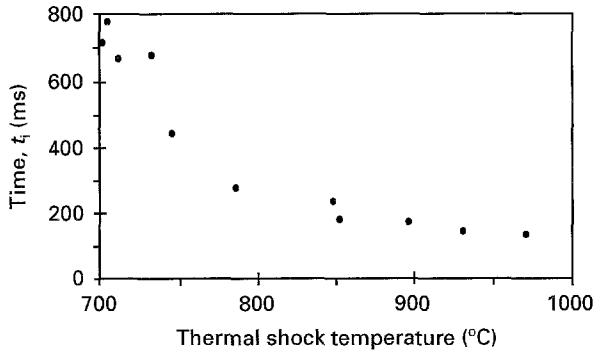

Figure 5 Evolution of the time needed to the apparition of the first crack as a function of the thermal shock temperature.

is lower than 1.5 s, which justifies a cooling time of 6 s in the thermal shock procedure. Note that the time to initiate the first acoustic peak, t_i, decreases rapidly when increasing thermal shock temperature. The evolution of t_i as a function of thermal shock temperature is represented in Fig. 5. These particular times t_i are quite interesting because at this instant they correspond to the onset of propagation of a single crack and therefore to a stress state that can be precisely calculated. It must be emphasized that these t_i values correspond to the instant of the first unstable crack propagation and are therefore of major interest.

4. Thermal shock behaviour

4.1. Numerical analysis

From the temperature field distribution $T(x, y)$ determined at the instant of the first cracking, the stress field $\sigma(x, y)$ was evaluated by finite element calculations. In this case the evolution of the elastic

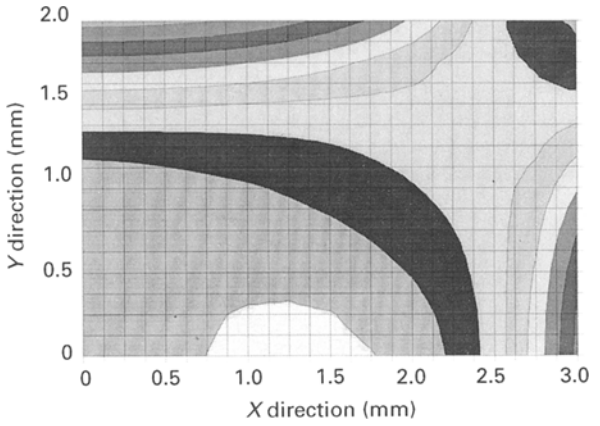

Figure 6 Maximal principal stress field induced by thermal shock for a temperature difference of 700 °C after 700 ms of cooling. 105–120; 90–105; 75–90; 60–75; 45–60; 30–45; 15–30; 0–15; – 15–30; – 30–45.

modulus and the coefficient of linear thermal expansion with temperature was taken into account. For example, the maximum principal stress field calculated for a temperature difference of 682 °C (i.e. corresponding to the critical temperature difference) at the instant of the first acoustic peak apparition t_i = 700 ms, is represented in Fig. 6. To summarize, we have a representation of the stress field at the instant of cracking for the given thermal shock condition. Note that the maximum stress is obtained on the surface of the largest face of the specimen. This surface stress was found to be 115 MPa for a temperature difference of 682 °C after 700 ms of cooling, which corresponds to the bending strength measured at 600 °C. Note also that the maximum stresses are located in the middle of the faces of the specimen and that angles of the specimens that generally contain higher defect concentrations are submitted to lower stresses. In order to confirm this theoretical result, thermal shock tests were conducted on a dense material (Mg-PSZ) where cracks could be easily observed with a dye penetrant. The failure was always observed exactly in the middle of the largest side of the specimen. In these conditions the thermal shock device generates a very well determined stress field, i.e. the stress field can be evaluated at any point of the specimen and any cooling time. For further analysis, only the maximum stress field $\sigma_{xx}(y, t)$ corresponding to the crack location will be taken into account, as shown in Fig. 7.

The stress intensity factor induced by thermal shock on open defects was calculated from a mono-dimensional model [6]. Considering the stress field $\sigma_{xx}(y, t)$ the evolution of the stress intensity factor can be evaluated as a function of the y axis, i.e. the size of the defect, at any cooling duration $K_I(y, t)$. A representation of the evolution of the stress intensity factor corresponding to a temperature of 700 °C as a function of cooling time and defect size is given in Fig. 8. We observe that the highest K-curve is reached after a cooling time of 700 ms, which corresponds to the appearance of the acoustic emission in such a thermal shock test condition.

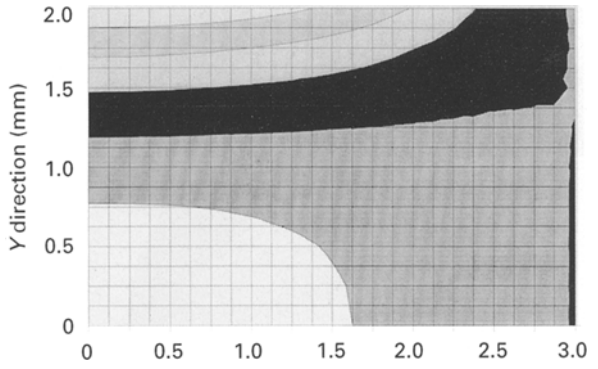

Figure 7 Stress field $\sigma_{xx}(Y)$ induced by thermal shock for a temperature of 700 °C after 700 ms of cooling. ▩ 90–120; ▩ 60–90; ▩ 30–60; ■ 0–30; ▩ – 30–60; □ – 60–90.

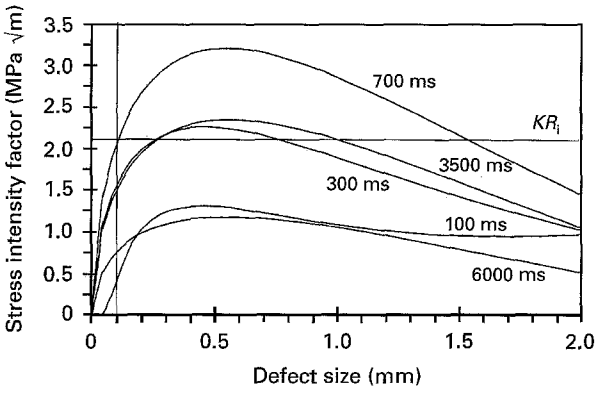

Figure 8 Stress intensity factor as a function of defect size and cooling time for a thermal shock temperature of 700 °C.

4.2. Analysis of results

The maximum thermal stress calculated at the instant of the first crack apparition can be compared to the strength measured by a four-point bending test. Note the close fit between these two data, which confirms the accuracy of the theoretical analysis and measurements. The same comparison can be advantageously conducted in terms of stress intensity factor. For this purpose, the resistance to crack propagation and the flaw distribution area of the material are also represented in Fig. 8. When the cooling time is increased K-curves also increase up to a maximum value at 700 ms. At this instant it is observed that the K-curve reaches the KR-curve of the material in the domain of the flaw size distribution. As a consequence the largest defect propagates in an unstable way and the acoustic emission of the material appears as shown in Fig. 4(a). In the present approach, the fracture behaviour is closely controlled by the resistance to crack propagation of the material.

Different stress intensity factor curves at the t_i instants corresponding to various thermal shock temperature differences were also calculated (Fig. 9). These K-curves correspond to the instants of cracking experimentally determined for several temperature differences. In Fig. 9, the first number indicates the thermal shock temperature difference ΔT and the second one the time required for the first unstable crack propagation: t_i. Note that for the lowest temperatures

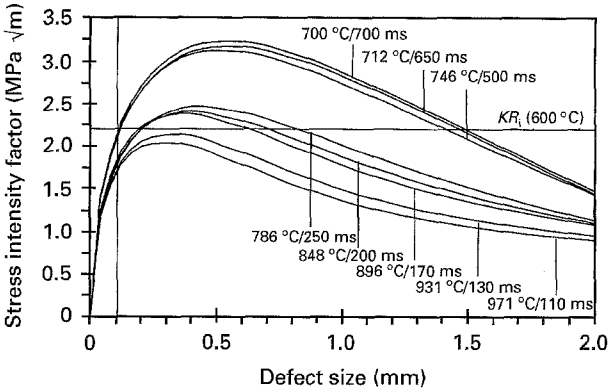

Figure 9 Stress intensity factor at t_i for various thermal shock temperature.

(700, 712 and 746 °C), which are near the critical temperature difference, the intercept of the K-curves with the initial KR value occurs for a defect size of 100 μm, which corresponds to the flaw size of the material previously measured. This suggests that for these thermal shock test conditions, the damage criteria are correctly identified. For the highest thermal shock temperature differences (786 to 971 °C), the K-curves intercept the critical size defect for lower value of KR, suggesting an error in the evaluation. This can however be explained by the fact that the initial value of the KR-curve decreases with increasing temperature, and also by the fact that the measurement of the instant of the first crack propagation t_i, becomes less precise when its value decreases.

It should be noted that in order to propose an extended analysis, the influence of a rising R-curve behaviour has been taken into account here. The R-curve of the presented alumina was shown not to be strongly significant for the thermal shock analysis. Its effects on subcritical crack growth and thermal fatigue are, however, strongly pronounced and will be discussed in further papers.

5. Conclusions

The present technique of thermal shock measurement and the use of a refined analysis which takes into account the whole thermal and mechanical properties allow a very good correlation between experimental results and prediction of thermal shock damage of alumina. Within these conditions, the conducted analysis has been strongly validated and the parameters controlling thermal shock behaviour clearly identified. It has been shown that the crack initiation induced by thermal shock is controlled by KR_i.

Thermal shock analysis can also be extended to real applications by simply adjusting the temperature and stress calculations to the component shape.

Acknowledgements

This work was supported by the department of advanced material (EMA) of Electricité de France (EDF). The authors wish to gratefully acknowledge Dr R. Rezakhanlou for this support.

References

1. F. MIGNARD, C. OLAGNON, G. FANTOZZI, P. CHANTRENNE and M. RAYNAUD, *J. Mater. Sci.*, in press.
2. J. B. WATCHMAN Jr and D. G. LAM Jr in "Alumina as a ceramic material", (American Ceramic Society, 1971) p. 53.
3. R. M. SPRIGGS and L. A. BRISSETTE, in "Alumina as a ceramic material", (American Ceramic Society, 1971) p. 54.
4. S. SAKAGUCHI, N. MURAYAMA, Y. KODAMA and F. WAKAI, *J. Mater. Sci. Lett.* **10** (1991) 282.
5. H. TADA, P. C. PARIS and G. R. IRWIN, "The stress analysis of cracks handbook", 2nd edition (Del Research Corporation, St Louis, MS, 1985) p. 2.13.
6. X. R. WU, "Thermal shock and thermal fatigue behaviour of advanced ceramics", edited by G. A. Schneider (Petzow, Germany, 1992) p. 119.

Received 4 October 1994
and accepted 9 November 1995